Electronic Supplementary Information for

$Cr_2O_7^{2-}$ inside Zr/Hf-Based Metal−Organic Frameworks: Highly Sensitive and Selective Detection and Crystallograghic Evidence

Kun Wu,[a] Ji Zheng,[a] Yong-Liang Huang,[b] Dong Luo,[a] Yan Yan Li,[a] Weigang Lu*[a] and Dan Li*[a]

[a] College of Chemistry and Materials Science, and Guangdong Provincial Key Laboratory of Functional Supramolecular Coordination Materials and Applications, Jinan University, Guangzhou 510632, P. R. China E-mail: weiganglu@jnu.edu.cn; danli@jnu.edu.cn

[b] Department of Chemistry, Shantou University Medical College, Shantou 515041, P. R. China

Contents

Section 1. Structural analysis

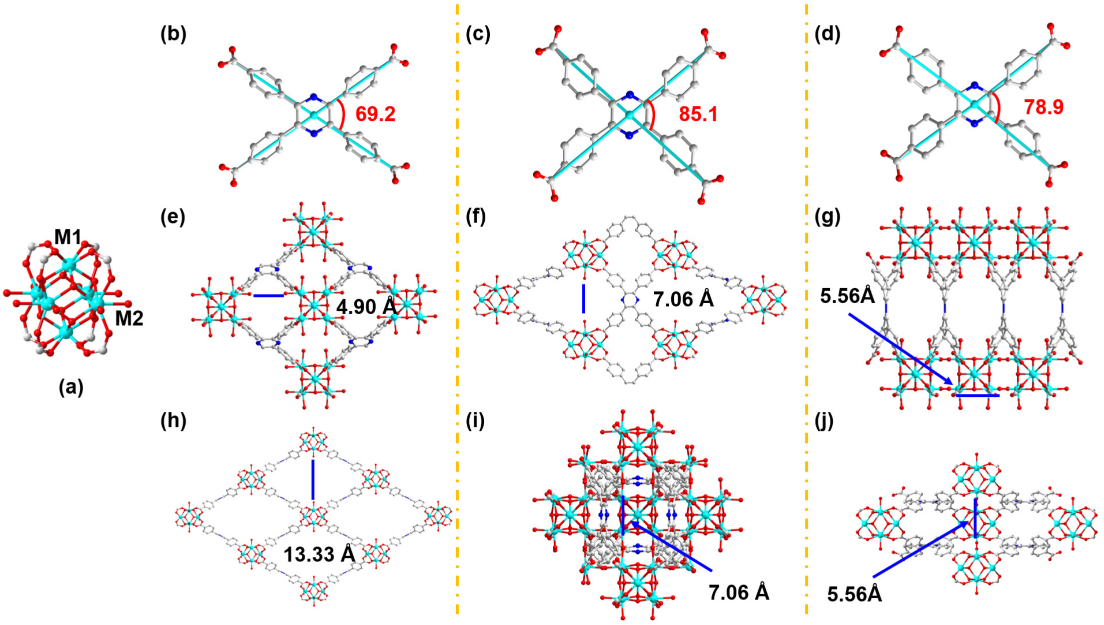

Fig. S1. Representation of the crystal structures of Zr/Hf-MOF-1, -2 and -3. (a) The cluster of Zr/Hf-O. The different torsional angles of the linkers in (b) Zr/Hf-MOF-1, (c) Zr/Hf-MOF-2, and (d) Zr/Hf-MOF-3. Crystal structures of (e) Zr/Hf-MOF-1, (f) Zr/Hf-MOF-2, and (g) Zr/Hf-MOF-3 viewed along [010] direction. Crystal structures of (h) Zr/Hf-MOF-1, (i) Zr/Hf-MOF-2, and (j) Zr/Hf-MOF-3 viewed along [001] direction.

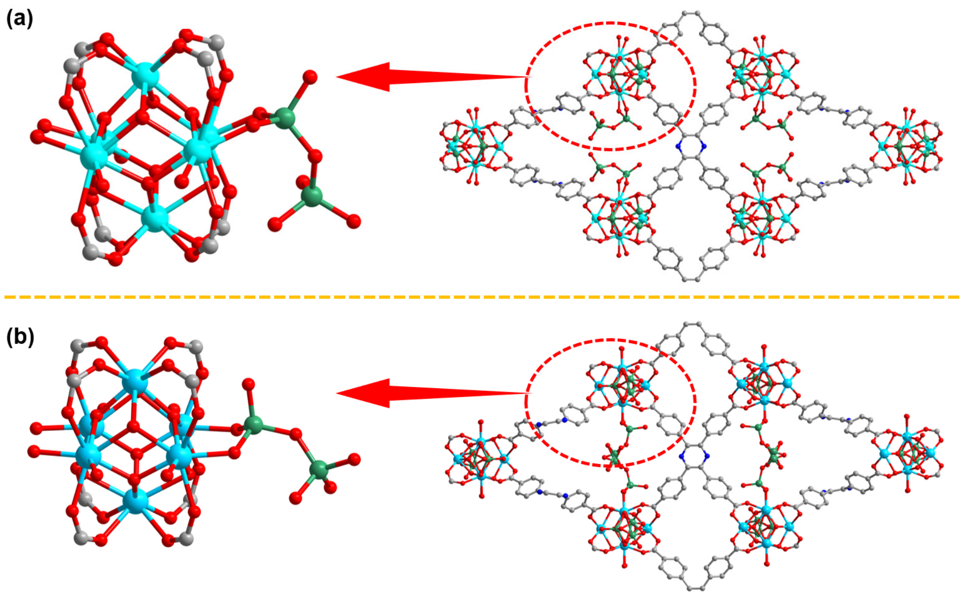

Fig. S2. Representation of the coordination environments of Zr_6/Hf_6 clusters in Zr/Hf-MOF-2-$Cr_2O_7^{2-}$ viewed along [010] direction, (a) Zr-MOF-2-$Cr_2O_7^{2-}$ and (b) Hf-MOF-2-$Cr_2O_7^{2-}$. (Colour code: C, gray; O, red; and Zr, turquoise; Zr, shy blue; Cr, green; One set of disorder $Cr_2O_7^{2-}$ and H atoms are omitted in each structure for clarity).

Section 2. Synthesis of H_4BTTB

4,4′,4″,4‴benzene-1,2,4,5-tetrayltetrabenzoic acid (short for H_4BTTB).[1]

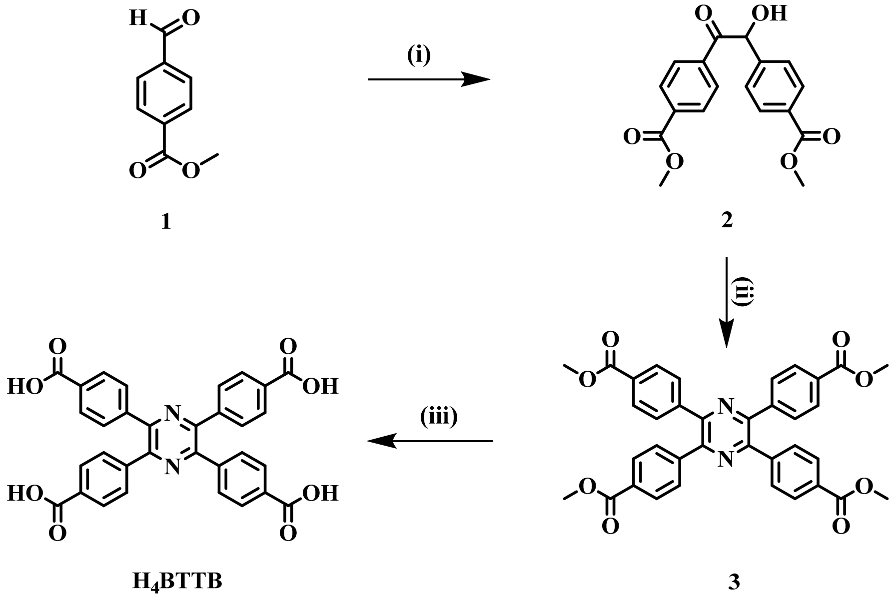

Scheme S1. The synthesis of ligand H_4BTTB: (i) MeOH, H_2O, VB_1, 2M NaOH; (ii) CH_3COOH, $(CH_3CO)_2O$, CH_3COONH_4; (iii) NaOH, THF/H_2O.

Synthesis of 2

To a solution of VB_1 (6.0 g, 20 mmol) in the mixed solvent of CH_3OH (90 mL) and H_2O (30 mL), add NaOH (16.6 mL, 2 M) dropwise to adjust the pH to 9−10. then **1** (50.0 g, 305 mmol) was added. The resulting mixture was stirred for 1 h in ice bath, then it was heated at 60 °C for 1 h and at 85 °C for 3 h. The precipitate was filtered to produce **2**. ^{1}H NMR (400 MHz, $CDCl_3$): δ = 8.08 (dt, 2H), 8.01 (dt, 2H), δ = 7.95 (dt, 2H), δ = 7.42 (dt, 2H), δ = 3.94 (s, 3H), δ = 3.90 (s, 3H).

Synthesis of 3

To a solution of **2** (30.1 g, 91.7 mmol) and CH_3COONH_4 (12 g, 155.7 mmol) in 90 mL of CH_3COOH, add acetic anhydride (9 mL, 91.7 mmol). After being stirred for 12 h at 120 °C under N_2, the dark orange precipitate was filtered and washed with diethyl ether to afford **3** (20.0? g, 32.5 mmol). ^{1}H NMR (400 MHz, $CDCl_3$): δ = 8.03 (d, 8H), 7.71 (d, 8H), 3.96 (s, 12H).

Synthesis of H_4BTTB

To a solution of **3** (20.0 g, 32.5 mmol) in THF/H_2O (1:1, 250 mL), add NaOH (20.0 g, 500. mmol), the resulting mixture was refluxed for 12 h. THF was removed in vacuum, and the remaining solution was acidified to pH of ca. 3 with HCl (2.0 M). The precipitate was filtered and washed with distilled water to afford H_4BTTB as a light-yellow solid (16.18 g, 28.9 mmol). ^{1}H NMR (400 MHz, DMSO-d6): δ = 13.10 (br, 4H), 7.94 (d, J = 8.4 Hz, 8H), 7.68 (d, J = 8.4 Hz, 8H). IR (cm−1): 3453(w), 3002(m), 2657(w), 2526(w), 1941(w), 1702(s), 1608(m), 1569(m), 1511(m), 1388(3), 1317(w), 1176(m), 1010(m), 1106(m), 860(m), 775(m), 717(m), 622(w), 543(m).

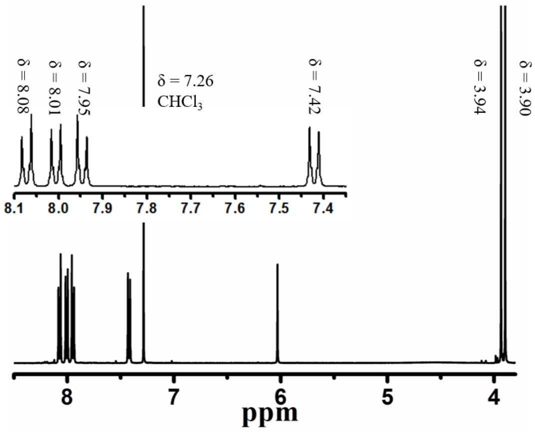

Fig. S3. ^{1}H NMR of **2**.

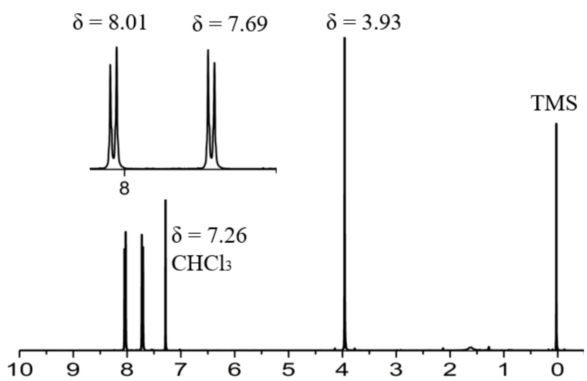

Fig. S4. ^{1}H NMR of **3**.

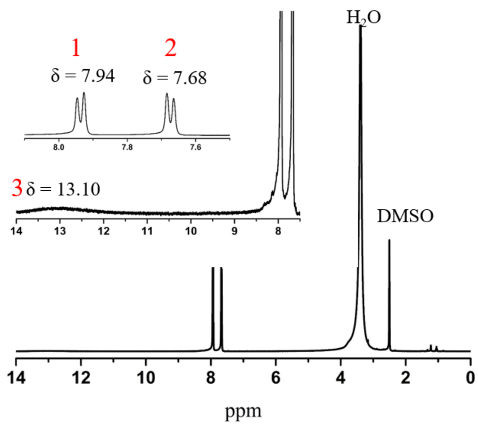

Fig. S5. ^{1}H NMR of H_4BTTB.

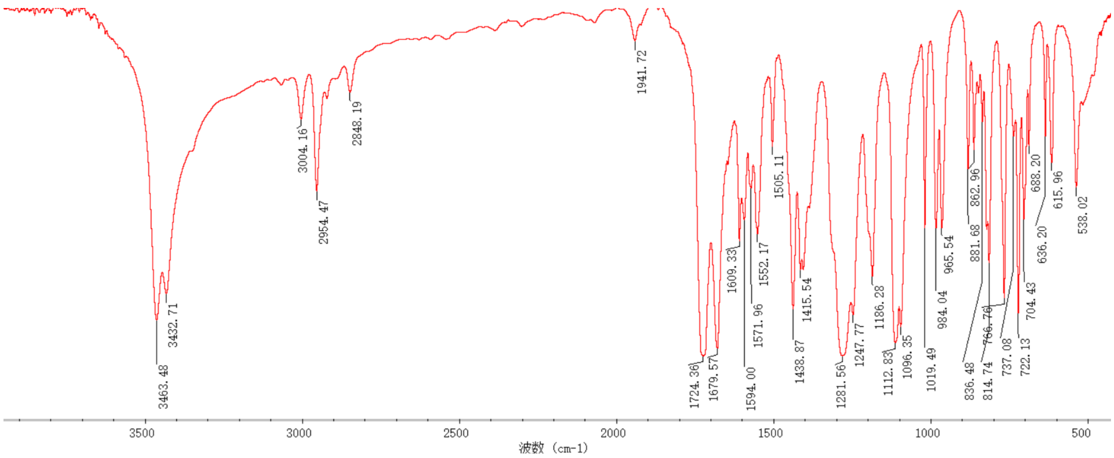

Fig. S6. FT-IR spectra of **2**.

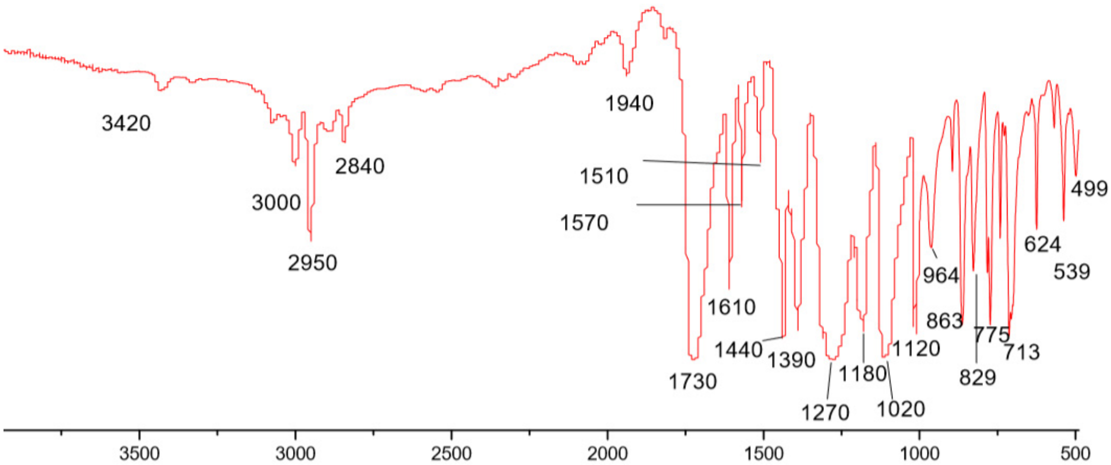

Fig. S7. FT-IR spectra of **3**.

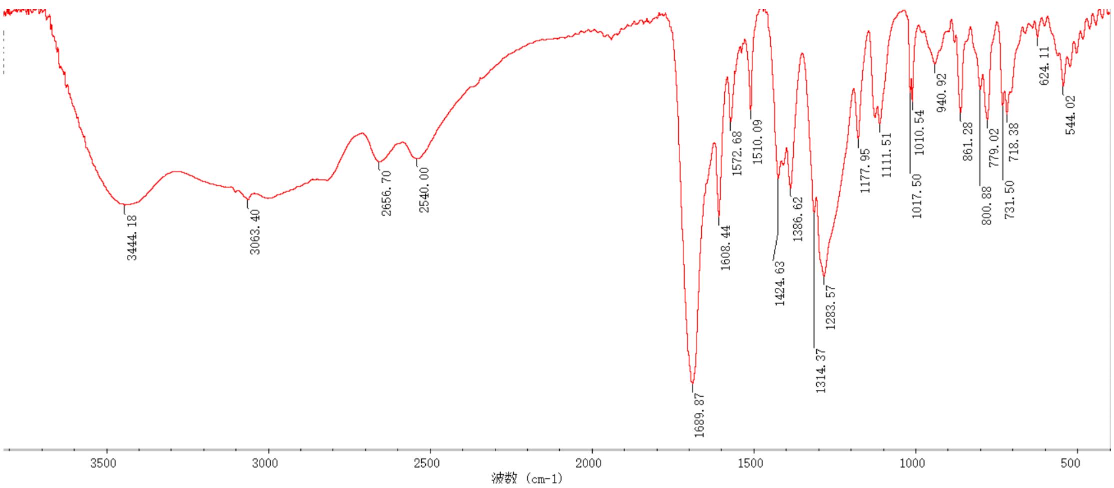

Fig. S8. FT-IR spectra of H_4BTTB.

Synthesis of Hf-MOF-1

Hf-MOF-1 was obtained through the solvothermal reaction of $HfCl_4$ (432 mg, 1.35 mmol) and H_4BTTB (200 mg, 0.035 mmol) in DMF (300 mL) in the presence of benzoic acid (34 g, 0.278 mmol) for 3 days at 120 °C. The mixture was then cooled down to room temperature. Colourless microcrystals were obtained and filtered, washed with solvents (DMF and acetone), and dried in an oven at 80 °C (yield 50%, based on H_4BTTB). Elemental analysis (%) for Hf-MOF-1: C, 40.79; H, 3.25; N, 3.39, found: C, 40.23; H, 3.31; N, 3.51.

Synthesis of Zr-MOF-1

Zr-MOF-1 was obtained through the reaction of $Zr(NO_3)_4 \cdot 5H_2O$ (580 mg, 1.35 mmol) and H_4BTTB (400 mg, 0.71 mmol) in DMF (150 mL) in the presence of HCOOH (140mL) for 3 days at 140 °C. The mixture was then cooled down to room temperature. Colourless microcrystals were obtained and filtered, washed with solvents (DMF and acetone), and dried in an oven at 80 °C (62%, based on H_4BTTB). Elemental analysis (%) for Zr-MOF-1: C, 44.78; H, 2.832; N, 2.7, found: C, 45.17; H, 3.07; N, 2.91. The same crystal structure has been previously reported.[2]

Synthesis of Zr-MOF-2

A mixture of $ZrOCl_2 \cdot 8H_2O$ (2.250 g, 6.98 mmol), H_4BTTB (1.245 g, 2.22 mmol), and DMF/HCOOH (870mL, 15/14, v/v) were added in a round-bottomed flask and heated in an oil bath (without stirring) under reflux at 130 °C for 72 h. After cooling to room temperature, the white polyhedron single crystals were obtained by filtration and washed with DMF 3 times (20.0 mL each time. Then, the crystals were soaked in acetone (40 mL) for 3 days at room temperature, when fresh solvents were exchanged every 8 h. The sample was collected by filtration and dried in air (yield 65%, based on H_4BTTB), which was determined as $[Zr_6(\mu_3\text{-}O)_4(\mu_3\text{-}OH)_4(OH)_4(H_2O)_4(BTTB)_2]$. Elemental analysis (%) for Zr-MOF-2: C, 43.09; H, 5.06; N, 4.41; found: C, 43.18; H, 5.10; N, 4.49. The same crystal structure has been previously reported.[2-4]

Synthesis of Zr-MOF-2′

To the filtrate of the mother liquor from the synthesis of Zr-MOF-2, add $ZrOCl_2 \cdot 8H_2O$ (2.250 g, 6.98 mmol) and H_4BTTB (1.245 g, 2.22 mmol). the resulting mixture was subjected to the same reaction condition and workup as for Zr-MOF-2. Microcrystalline Zr-MOF-2′ was obtained (yield 68%, based on H_4BTTB). PXRD studies indicated that Zr-MOF-2′ has the same structure as Zr-MOF-2. Notably, the DMF/HCOOH filtrate can be recycled to produce microcrystalline Zr-MOF-2′ several times with good yields.

Synthesis of Zr-MOF-2-$Cr_2O_7^{2-}$ The as-synthesized Zr-MOF-2 samples (20 mg) were soaked in 5mM $Cr_2O_7^{2-}$ aqueous solutions at room temperature for 4 d. Then, the samples were collected by filtration, washed with water before SCXRD and PXRD investigations.

Synthesis of Hf-MOF-3

$HfOCl_2 \cdot 8H_2O$ (51 mg, 0.124 mmol), H_4BTTB (100 mg, 0.179 mmol), DMF (15 mL), and HCOOH (14 mL) were added into a round-bottomed flask and heated in an oil bath (no stirring) under reflux at 130 °C for 7 d. After cooling to room temperature, the white polyhedron single crystals were obtained by filtration and washed with DMF for 3 times. Then, the crystals were soaked in acetone (40 mL) for 3 days at room temperature. The sample was collected by filtration and dried in air (yield 53%, based on H_4BTTB), which was determined as $[Hf_6(\mu_3\text{-}O)_4(\mu_3\text{-}OH)_4 (OH)_4 (H_2O)_4 (BTTB)_2]\cdot 9$ DMF·3.5 H_2O. Elemental analysis (%) for Hf-MOF-3: C, 43.24; H, 5.10; N, 4.52; found: C, 43.50; H, 5.17; N, 4.61.

Synthesis of Zr-MOF-3

A mixture of $ZrOCl_2\cdot 8H_2O$ (40 mg, 0.124 mmol), H_4BTTB (100 mg, 0.179 mmol), DMF (15 mL), and HCOOH (14mL) was added into a round-bottomed flask and heated in an oil bath (no stirring) under reflux at 130 °C for 7 d. After cooling to room temperature, colourless single crystals were obtained by filtration and washed with DMF 3 times. Then, the crystals were soaked in acetone (40 mL) for 3 days at room temperature. The sample was collected by filtration and dried in air (yield 60%, based on H_4BTTB), which was determined as $[Zr_6(\mu_3\text{-}O)_4(\mu_3\text{-}OH)_4 (OH)_4 (H_2O)_4 (BTTB)_2]\cdot 9$ DMF·3.5 H_2O. Elemental analysis (%) for Zr-MOF-3 calculated: C, 43.4; H, 3.425; N, 2.52; found: C, 43.05; H, 3.61; N, 2.64. The crystal structure has been previously reported.[4]

Determination of the Crystal Structures

Single-crystal X-ray diffraction data of Hf-MOF-2, Hf-MOF-3, Zr-MOF-2, Zr-MOF-3, Zr-MOF-2-$Cr_2O_7^{2-}$and Hf-MOF-2-$Cr_2O_7^{2-}$ were collected *via* an Oxford Cryo stream system on a XtaLAB PRO MM007-DW diffractometer system equipped with a RA-Micro7HF-MR-DW(Cu/Mo) X-ray generator and Pilatus3R-200K-A detector (Rigaku, Japan, Cu Kα, λ = 1.54178 Å) at 100(2) K. The numerical absorption corrections were applied using the program of ABSCOR. The structures were solved using direct methods, which yielded the positions of all non-hydrogen atoms, and they were refined anisotropically. Hydrogen atoms were placed in calculated positions with fixed isotropic thermal parameters and included in the structure factor calculations in the final stage of full-matrix least-squares refinement. All calculations were performed using the SHELXTL system of computer programs. The unit cell volume included a large region of disordered solvent which could not be modelled as discrete atomic sites. The treatment for the guest molecules in the cavities of all crystals involves the use of the SQUEEZE program of PLATON. Crystal data and structure refinement parameters are summarized in Tables S2-S3. Topology information for the Zr/Hf-MOFs was calculated by TOPOS 4.0.35.

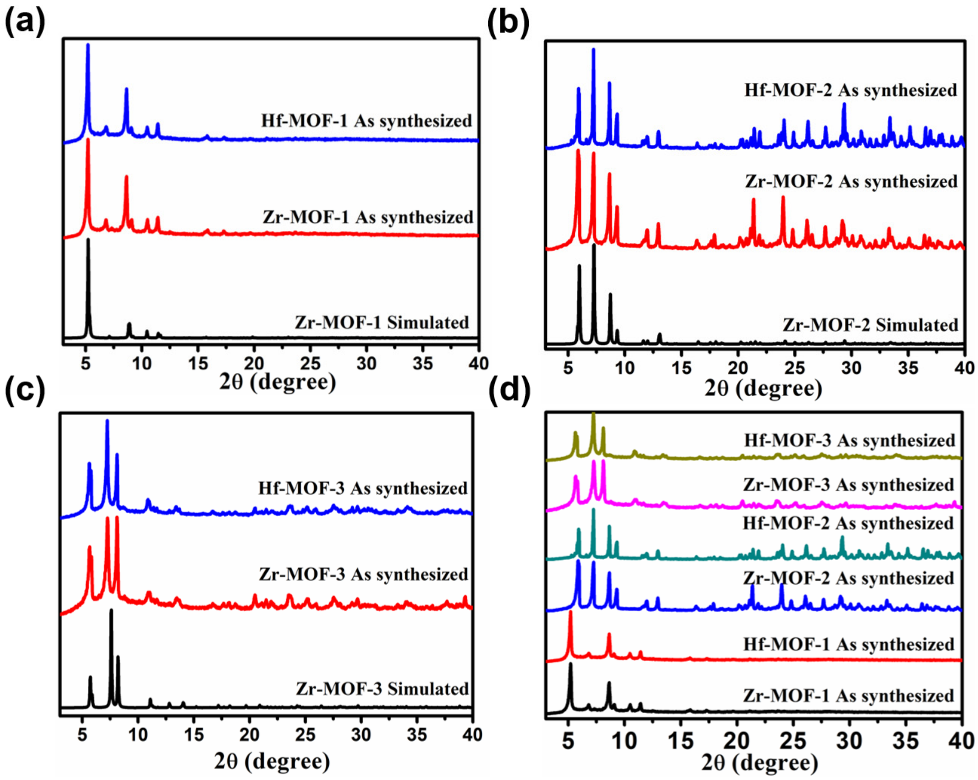

Fig. S9. PXRD patterns of (a) Zr/Hf-MOF-1, (b) Zr/Hf-MOF-2, and (c) Zr/Hf-MOF-3. (d) Comparison of PXRD patterns of the six as-synthesized MOFs.

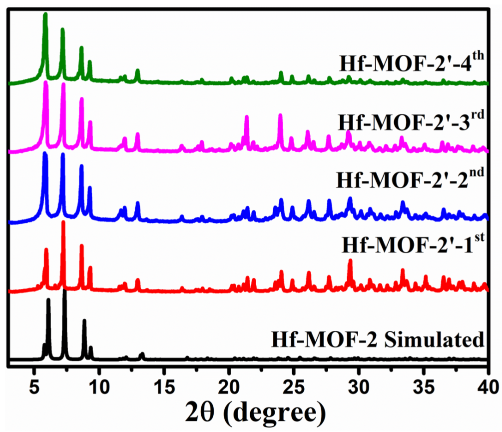

Fig. S10. Comparison of PXRD patterns of Hf-MOF-2 (simulated) and Hf-MOF-2′ (1st, 2nd, 3rd, 4th) synthesized with the recycled mother liquor four times.

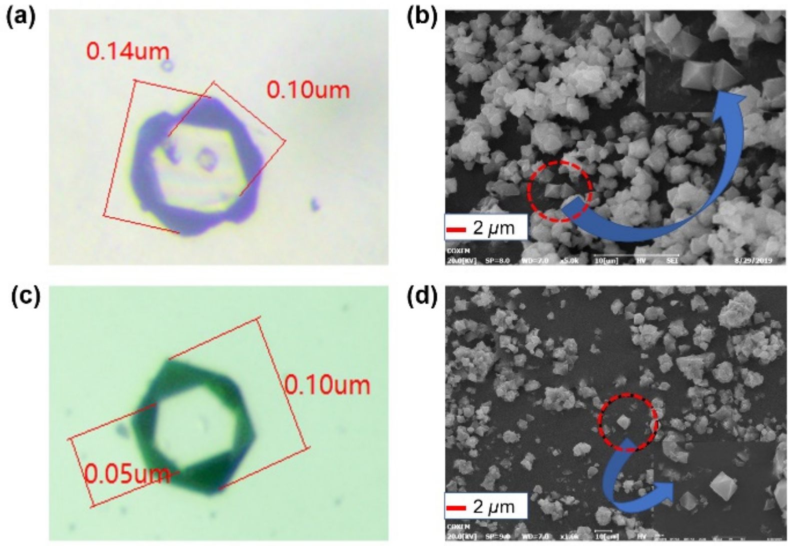

Fig. S11. Optical images of the (a) Hf-MOF-2 and (c) Zr-MOF-2. Desktop SEM images of (b) Hf-MOF-2′ and (d) Zr-MOF-2′.

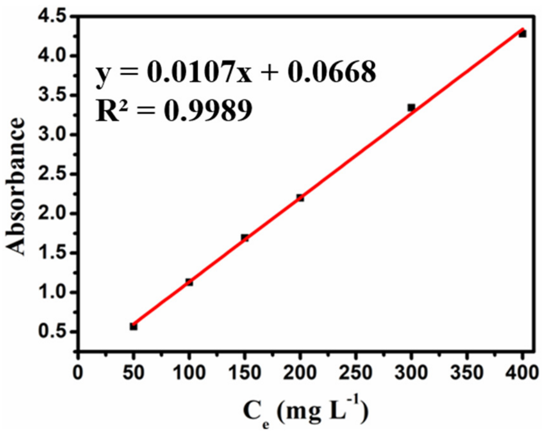

Fig. S12. UV-Vis absorption standard curve for $Cr_2O_7^{2-}$ in aqueous solution.

Section 3. Crystallographic data

Table S1. Crystal data and structure refinement for Hf-MOFs.

MOF	**Hf-MOF-2**	**Hf-MOF-3**	**Hf-MOF-2- $Cr_2O_7^{2-}$**
Empirical formula	$C_{32}H_{24}Hf_3N_2O_{16}$	$C_{32}H_{28}Hf_3N_2O_{16}$	$C_{32}H_{20}Cr_{0.75}Hf_3N_2O_{17.75}$
Formula weight	1228.00	1232	1290.97
Crystal system	tetragonal	orthorhombic	tetragonal
Space group	$I4_1/amd$	*Fmmm*	$I4_1/amd$
a/ Å	14.92550(10)	13.3952(3)	15.08800(10)
b/ Å	14.92550(10)	30.9940(4)	15.08800(10)
c/ Å	61.0560(6)	30.0265(4)	60.1315(10)
V/ $Å^3$	13601.5(2)	12466.1(4)	13688.8(3)
Z	8	8	8
D_C /g cm^{-3}	1.199	1.313	1.253
μ /mm^{-1}	8.593	9.376	9.503
λ / Å	1.54184	1.54184	1.54184
T/ K	100	100	100
Reflections collected	20579	11175	24012
Independent reflections	3879 [R_{int} = 0.0345]	3423 [R_{int} = 0.0418]	3844 [R_{int} = 0.0290]
Goodness-of-fit on F^2	1.073	1.090	1.139
R_1 [a], wR_2 [b] [I > 2σ (I)]	R_1 = 0.0345, wR_2 = 0.1098	R_1 = 0.0434, wR_2 = 0.1199	R_1 = 0.0464, wR_2 = 0.1398
R_1 [a], wR_2 [b] (all data)	R_1 = 0.0385, wR_2 = 0.1106	R_1 = 0.0456, wR_2 = 0.1222	R_1 = 0.0480, wR_2 = 0.1420
Largest diff. peak and hole /e.$Å^{-3}$	1.47/-1.76	3.46/-1.99	1.61/-1.54

[a] $R_1 = \Sigma||F_o|-|F_c|| / \Sigma|F_o|$

[b] $wR_2 = \{\Sigma[w(F_o^2 - F_c^2)^2]/[w(F_o^2)^2]\}^{1/2}$, $[F_o > 4\sigma(F_o)]$

Table S2. Crystal data and structure refinement for Zr-MOFs.

MOF	**Zr-MOF-2**	**Zr-MOF-3**	**Zr-MOF-2- $Cr_2O_7^{2-}$**
Empirical formula	$C_{32}H_{24}N_2O_{16}Zr_3$	$C_{32}H_{28}N_2O_{16}Zr_3$	$C_{32}H_{18}Cr_{0.75}N_2O_{17.15}Zr_3$
Formula weight	966.19	972.22	1017.54
Crystal system	tetragonal	orthorhombic	tetragonal
Space group	$I4_1/amd$	*Fmmm*	$I4_1/amd$
a/ Å	15.20200(10)	13.8240(3)	15.11968(7)
b/ Å	15.20200(10)	13.8240(3)	15.11968(7)
c/ Å	60.5990(8)	30.9041(6)	60.2341(5)
V/ Å ^{3}	14004.5(3)	12466.1(4)	13769.80(17)
Z	8	8	8
D_C /g cm $^{-3}$	1.874	1.004	0.982
μ /mm $^{-1}$	9.328	4.300	4.957
λ / Å	1.54184	1.54184	1.54184
T/ K	100	100	100
Reflections collected	16566	11989	44052
Independent reflections	3619 [R_{int} = 0.0248]	3122 [R_{int} = 0.0723]	3158 [R_{int} = 0.0299]
Goodness-of-fit on F ^{2}	1.086	1.090	1.123
R_1 ^{a}, wR_2 ^{b} [$I > 2\sigma(I)$]	R_1 = 0.0391, wR_2 = 0.1217	R_1 = 0.0669, wR_2 = 0.1856	*R1* = 0.0913, *wR2* = 0.3234
R_1 ^{a}, wR_2 ^{b} (all data)	R_1 = 0.0415, wR_2 = 0.1258	R_1 = 0.0722, wR_2 = 0.1903	*R1* = 0.0926, *wR2* = 0.3354
Largest diff. peak and hole /e.Å $^{-3}$	1.95/-0.79	2.23/-1.81	2.09/-1.35

[a] $R_1 = \Sigma||F_o|-|F_c|| / \Sigma|F_o|$

[b] $wR_2 = \{\Sigma[w(F_o{}^2 - F_c{}^2)^2]/[w(F_o{}^2)^2]\}$ 1/2 , [$F_o > 4\sigma(F_o)$]

Section 4. General characterizations

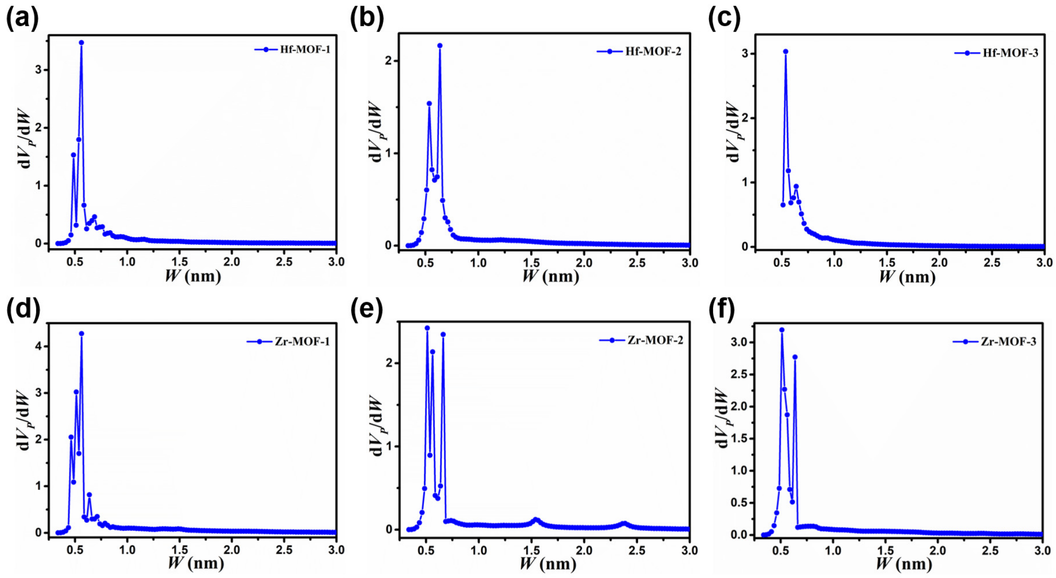

Fig. S13. Pore size distributions of (a) Hf-MOF-1, (b) Hf-MOF-2, (c) Hf-MOF-3, (d) Zr-MOF-1, (e) Zr-MOF-2, and (f) Zr-MOF-3.

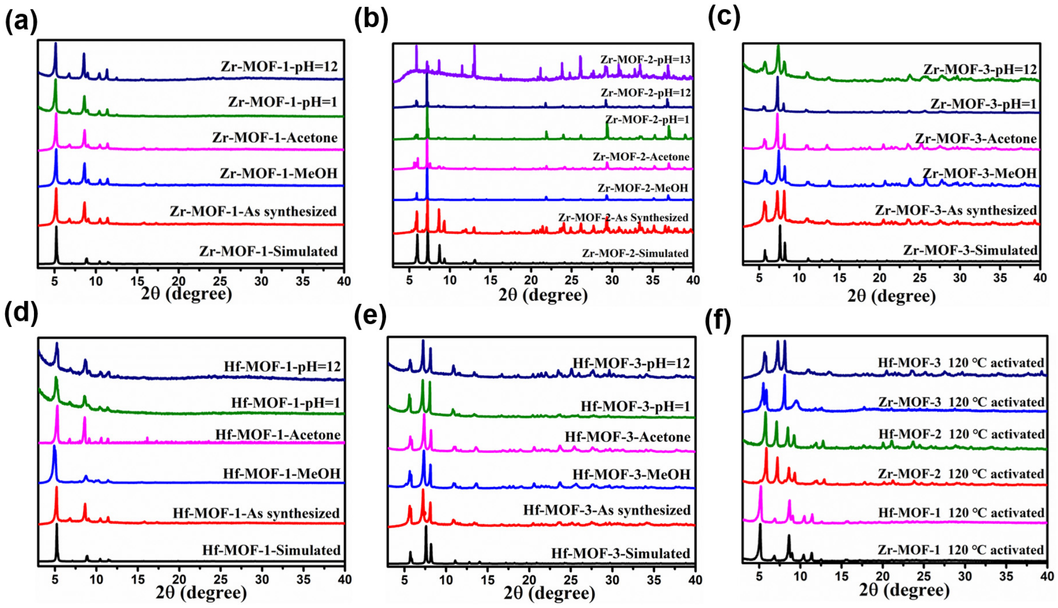

Fig. S14. PXRD patterns of Zr/Hf-MOFs (a-e) soaked in different organic solvents and treated with aqueous solutions at different pH values. (f) PXRD patterns of the MOFs activated overnight at 120 °C in a vacuum oven.

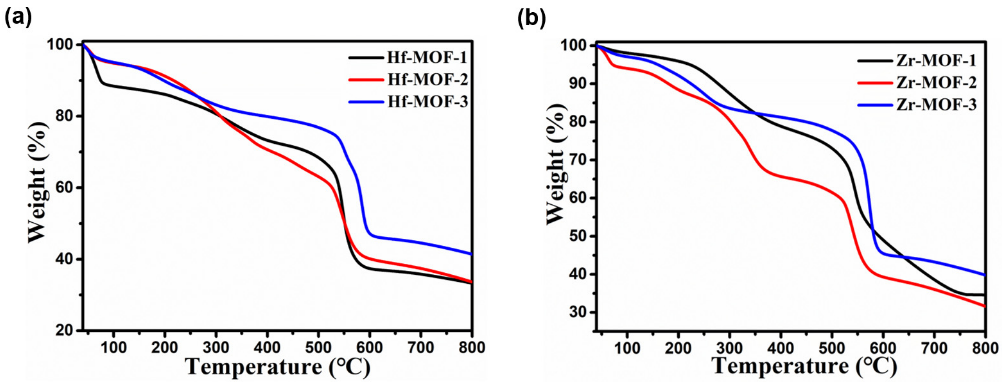

Fig. S15. Thermogravimetric analysis of (a) Hf-MOFs and (b) Zr-MOFs.

Section 5. Adsorption of $Cr_2O_7^{2-}$

Table S3. ICP-AES results[a] for Hf-MOF-2-$Cr_2O_7^{2-}$ and Zr-MOF-2-$Cr_2O_7^{2-}$.

		ρ(Hf/Zr) / ppm	ρ(Cr) / ppm	ratio
Hf-MOF-2-Cr	1	30.533	5.832	1.525
	2	36.153	7.093	1.485
	3	42.924	8.392	1.490
Zr-MOF-2-Cr	1	23.876	7.108	1.915
	2	27.467	8.080	1.938

[a] All data are from different batches of prepared samples to ensure the reproducibility

Table S4. Comparison of detection and adsorption capacities for $Cr_2O_7^{2-}$ of selected porous materials.

MOF Adsorbents	Maximum Capacity (mg /g)	The SC-to SC process	Recyclability	Quenching constant(M^{-1})	LOD (μM)	Reference
Hf-MOF-3	32	No	Yes	4.51×10^5	0.013	This work
Zr-MOF-3	30	No	Yes	6.37×10^5	0.019	This work
Hf-MOF-2	153	Yes	Yes	4.56×10^4	0.188	This work
Zr-MOF-2	149	Yes	Yes	3.5×10^4	0.244	This work
Hf-MOF-1	27	No	Yes	7.1×10^4	0.138	This work
Zr-MOF-1	28	No	Yes	6.2×10^4	0.138	This work
3D Ag-based MOF	0.73 mol/mol	Yes	NA	NA	NA	*Angew. Chem. Int. Ed.*, 2013, 52, 13769–13773.
FIR-53	74.2	Yes	NA	NA	NA	*Chem. Mater.*, 2015, **27**, 205–210.
1-Br	128	Yes	NA	NA	NA	*Chem. Commun.*, 2017, **53**, 1860–1863.
ZJU-101	245	No	Yes	NA	NA	*Chem. Commun.*, 2015, **51**, 14732–14734.
TJNU-244	269	Yes	Yes	NA	NA	*ACS Appl. Mater. Interfaces*, 2019, **11**, 42375–42384.
TJNU-243	273	Yes	Yes	NA	NA	*ACS Appl. Mater. Interfaces*, 2019, **11**, 42375–42384.
TJNU-334	293	Yes	Yes	NA	NA	*ACS Appl. Mater. Interfaces*, 2019, **11**, 42375–42384.
JLU-MOF50	92	No	Yes	4.99×10^4	NA	*J. Mater. Chem. A*, 2018, **6**, 6363-6369.
BUT-39	215	No	Yes	1.57×10^4	1.5	*ACS Appl. Mater. Interfaces* 2018, **10**, 16650−16659.
Zr-BDC-$(NH_2)_2$	303	No	Yes	NA	NA	*J. Mater. Chem. A*, 2020, **8**, 9629-9637.

Zr-BDC-(NH2)2@PB	208	No	Yes	NA	NA	*J. Mater. Chem. A*, 2020, **8**, 9629-9637.
NU-1000	76.80	No	Yes	1.34×10^4	1.8	*Inorg. Chem.,* 2017, **56**, 14178−14188.
Zn-MOF-1	NA	No	Yes	2.07×10^4	3.53	*J. Mater. Chem. A*, 2017, **5**, 20035–20043.
$[Zn_2(TPOM)(NDC)_2]\cdot 3.5H_2O$	NA	No	Yes	9.21×10^3	2.35	*Inorg. Chem.*, 2017, **56**, 12348-12356
$[Eu(ipbp)_2(H_2O)_3]Br\cdot 6H_2O$	NA	No	Yes	8.98×10^3	NA	*J. Mater. Chem. C*, 2017, **5**, 8999–9004.
BUT-28	NA	No	Yes	1.02×10^5	0.12	*Inorg. Chem.*, 2018, **57**, 14260−14268.
$[Y(BTC)(DMF)_6]_n$: 0.1Eu	NA	No	NA	4.52×10^3	0.04	*Microporous Mesoporous Mater.*, 2015, **217**, 196−202.
$[Zn(btz)]_n$	NA	No	Yes	4.23×10^3	2	*CrystEngComm*, 2016, **18**, 4445−4451.
$[Zn(ttz)\ H_2O]_n$	NA	No	Yes	2.19×10^3	2	*CrystEngComm*, 2016, 1**8**, 4445−4451.
$[Zn(IPA)(3\text{-}PN)]_n$	NA	No	Yes	1.37×10^3	12.02	*Inorg. Chem.*, 2017, **56**, 2627−2638.
$[Cd(IPA)(3\text{-}PN)]_n$	NA	No	Yes	2.91×10^3	2.26	*Inorg. Chem.*, 2017, **56**, 2627−2638.
$\{[Cd(4\text{-}BMPD)(BPDC)]\cdot 2H_2O\}_n$	NA	No	NA	6.4×10^3	37.6	*Cryst. Growth Des.*, 2017, **17**, 67−72.
$\{[Cd(4\text{-}BMPD)(SDBA)(H_2O)]\cdot 0.5H_2O\}n$	NA	No	NA	4.97×10^3	48.6	*Cryst. Growth Des.,* 2017, **17**, 67−72.
$[Eu_2(tpbpc)_4\cdot CO_3\cdot H_2O]\cdot$ DMF·solvent	NA	No	Yes	1.04×10^4	1.07	*Inorg. Chem.,* 2017, **56**, 4197−4205.
$[Tb(hfac)_3(NITPh\text{-}Pa)_2][0.5CH_3(CH_2)_5CH_3]$	NA	No	NA	1.98×10^4	0.01	*Polyhedron*, 2018, **144**, 101−106.
$[Ag(btx)_{0.5}(DCTP)_{0.5}]_n$	NA	No	NA	1.92×10^4	2.04	*J. Mol. Struct.*, 2018, **1155**, 496−502.
$[Zn(2\text{-}NH_2bdc)(bibp)]_n$	NA	No	NA	6.5×10^6	NA	*Inorg. Chem.*, 2015, **54**, 7133−7135.
$[Zn_2(tpeb)(bpdc)_2]$	NA	No	Yes	1.122×10^4	1.04	*Inorg. Chem.*, 2020, **59**, 8818−8826.
$Zr\text{-}BDC\text{-}(NH_2)_2$	303	No	Yes	NA	NA	*J. Mater. Chem. A*, 2020, **8**, 9629–9637.
$Zr\text{-}BDC\text{-}(NH_2)_2@PB$	432	No	Yes	NA	NA	*J. Mater. Chem. A*, 2020, **8**, 9629–9637
$[In_3(ipbp)_2(\mu_2\text{-}OH)(\mu_2\text{-}O)_3]$	74.4	No	Yes	NA	NA	*Dalton Trans.*, 2020, **49**, 10613–10620
UPC-48	62.9	No	Yes	NA	NA	*Chem. Commun.*, DOI: 10.1039/d0cc04007j
UPC-49	93.7	No	Yes	NA	NA	*Chem. Commun.*, DOI: 10.1039/d0cc04007j
UPC-50	61.8	No	Yes	NA	NA	*Chem. Commun.*, DOI: 10.1039/d0cc04007j

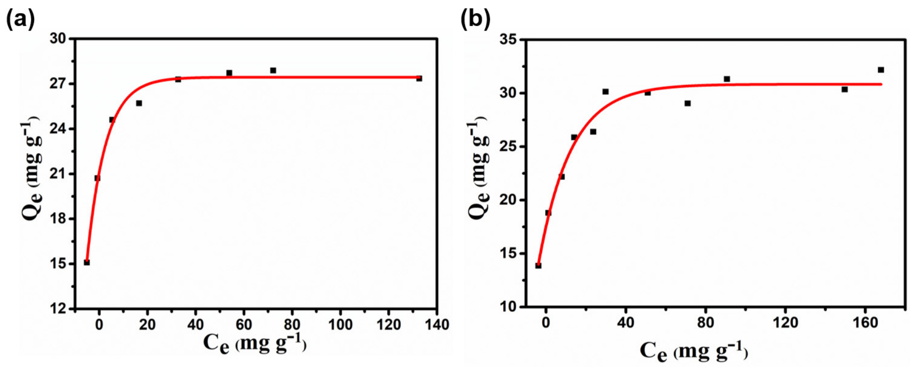

Fig. S16. Adsorption isotherm of $Cr_2O_7^{2-}$ in (a) Hf-MOF-1 and (b) Hf-MOF-3.

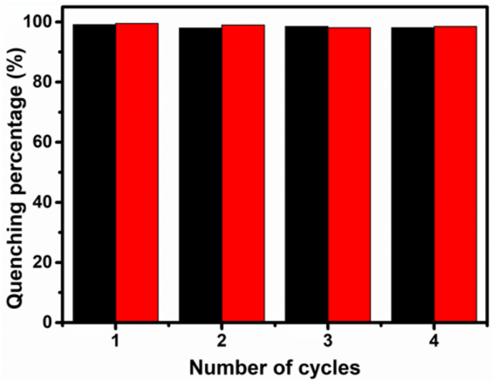

Fig. S17. The quenching efficiencies of Zr-MOF-2 (black) and Hf MOF-2 (red) suspensions in four regeneration cycles.

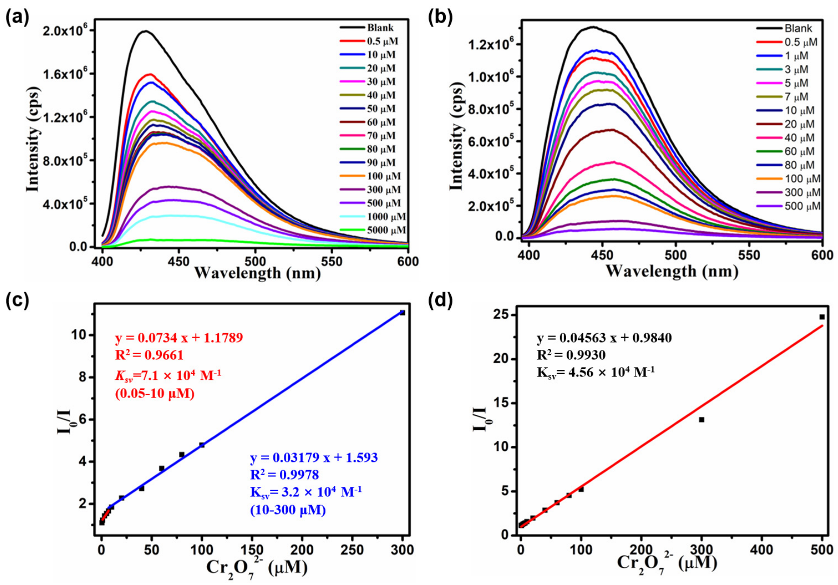

Fig. S18. Concentration-dependent luminescence emission spectra of (a) Hf-MOF-1 and (b) Hf-MOF-2 upon incremental addition of $Cr_2O_7^{2-}$ (0.5, 1, 2, 3, 4, 5, 6, 7, 8 9,10, 20, 40, 60, 80, 100 and 300 μM). Stern–Volmer (S–V) plot of I_0/I versus $Cr_2O_7^{2-}$concentration from 0.0 to 300 μM for (c) Hf-MOF-1 and (d) Hf-MOF-2.

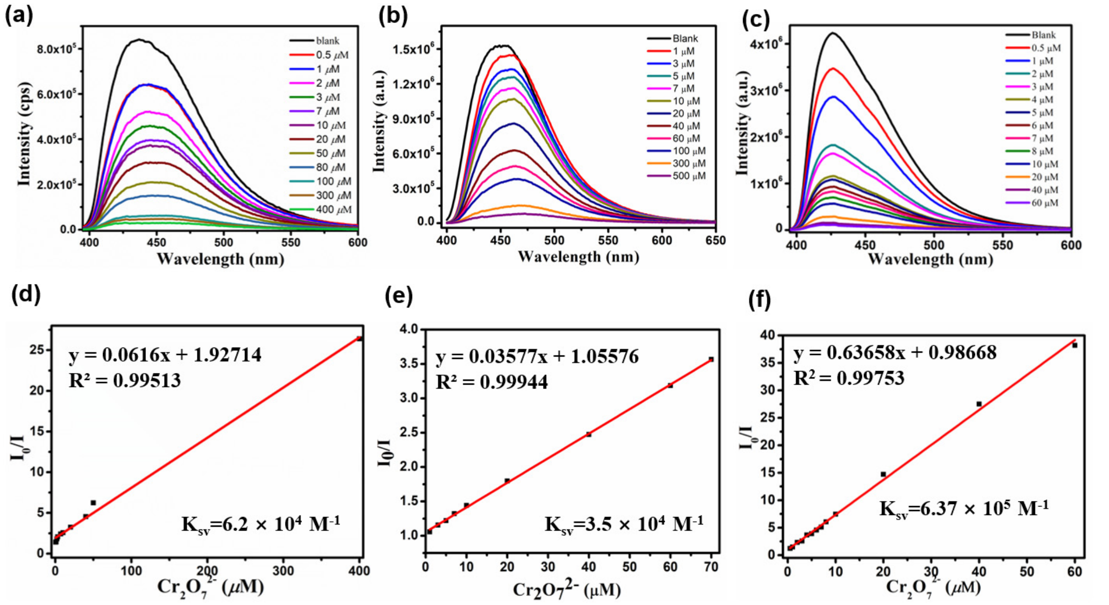

Fig. S19. Concentration-dependent luminescence emission spectra of (a) Zr-MOF-1, (b) Zr-MOF-2, and (c) Zr-MOF-3 upon incremental addition of $Cr_2O_7^{2-}$ (0.5, 1, 2, 3, 4, 5, 6, 7, 8 9,10, 20, 40, 60, 80, 100 and 300 μM). Stern–Volmer (S–V) plot of I_0/I versus $Cr_2O_7^{2-}$concentration from 0.0 to 300 μM for (d) Zr-MOF-1, (e) Zr-MOF-2, and (f) Zr-MOF-3.

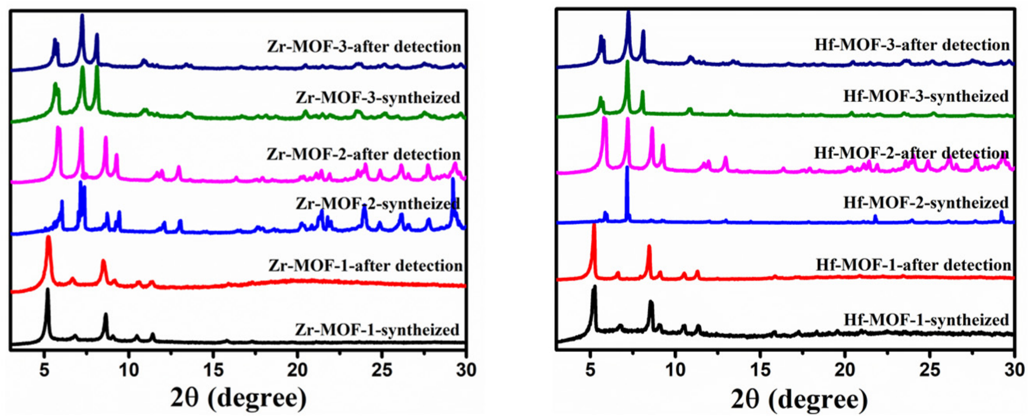

Fig. S20. PXRD patterns of Zr/Hf-MOFs before and after the detection of $Cr_2O_7^{2-}$.

Section 6. Detection of $Cr_2O_7^{2-}$

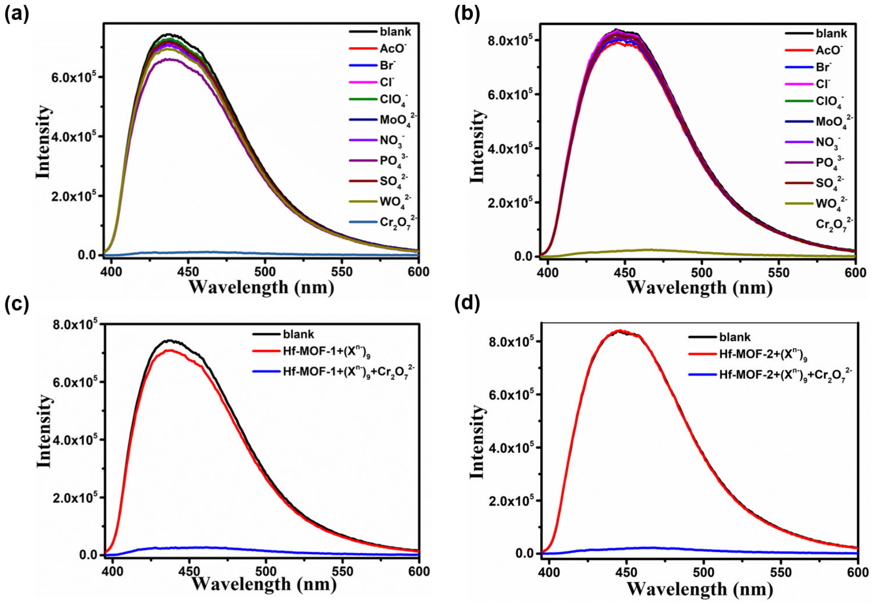

Fig. S21. Luminescent spectra of (a) Hf-MOF-1 and (b) Hf-MOF-2 suspensions in the presence of 0.5 mM different anions under excitation of 380 nm. Luminescent spectra of (c) Hf-MOF-1 and (d) and Hf-MOF-2 suspensions upon the addition of $Cr_2O_7^{2-}$ in the presence of nine anions (X = AcO^-, Br^-, Cl^-, ClO_4^-, MoO_4^{2-} NO_3^-, PO_4^{3-}, SO_4^{2-}, and WO_4^{2-}, 0.05 mM for each anion).

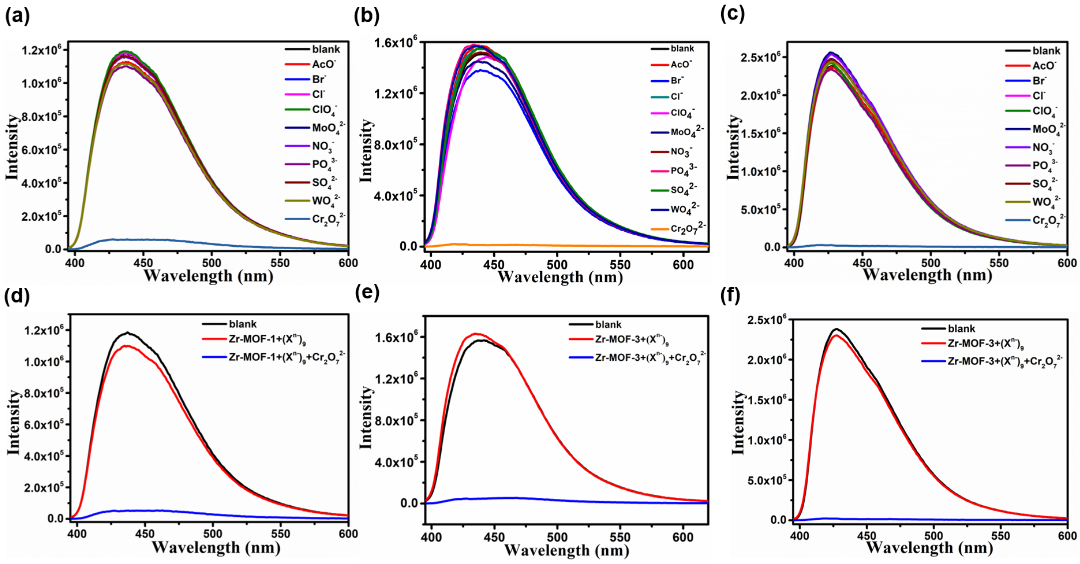

Fig. S22. Luminescent spectra of (a) Zr-MOF-1, (b) Zr-MOF-2, and (c) Zr-MOF-3 suspensions in the presence of 0.5 mM different anions under excitation of 380 nm. Luminescent spectra of (d) Zr-MOF-1, (e) Zr-MOF-2, and (f) Zr-MOF-3 upon the addition of $Cr_2O_7^{2-}$ in the presence of nine anions (X = AcO^-, Br^-, Cl^-, ClO_4^-, MoO_4^{2-} NO_3^-, PO_4^{3-}, SO_4^{2-}, and WO_4^{2-}, 0.05 mM for each anion).

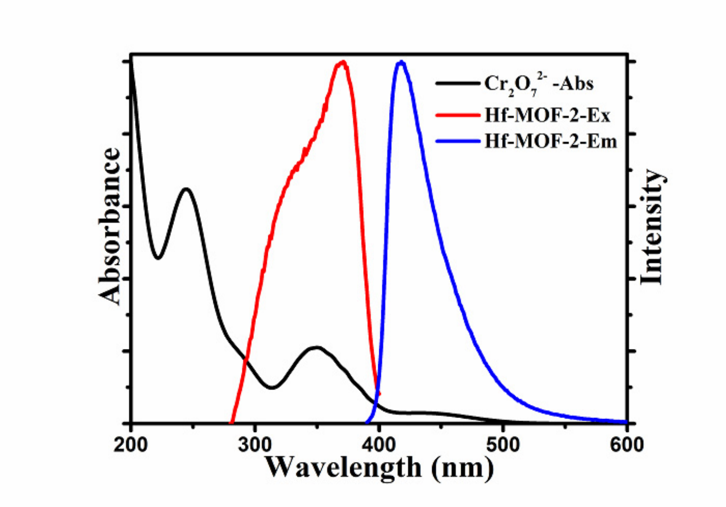

Fig. S23. Spectral overlap between the UV-vis absorption spectrum of $Cr_2O_7^{2-}$, excitation spectrum of Hf-MOF-2, and emission spectrum of Hf-MOF-2.

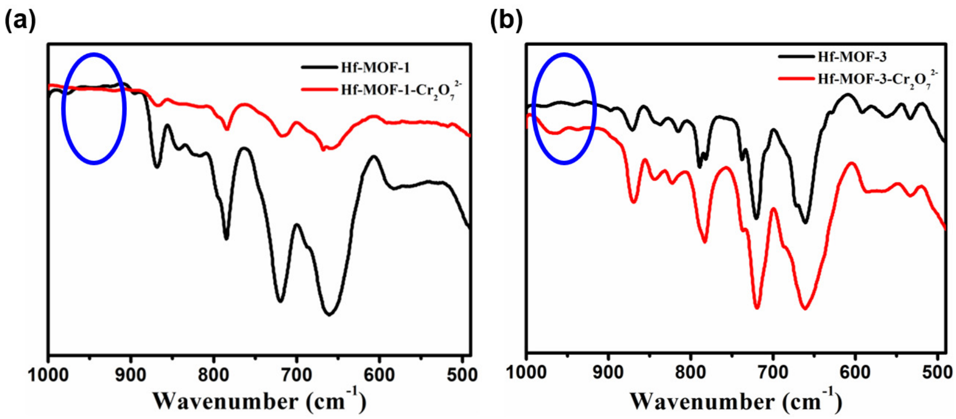

Fig. S24. FT-IR spectra of (a) Hf-MOF-1 and (b) Hf-MOF-3 before and after the adsorption of $Cr_2O_7^{2-}$.

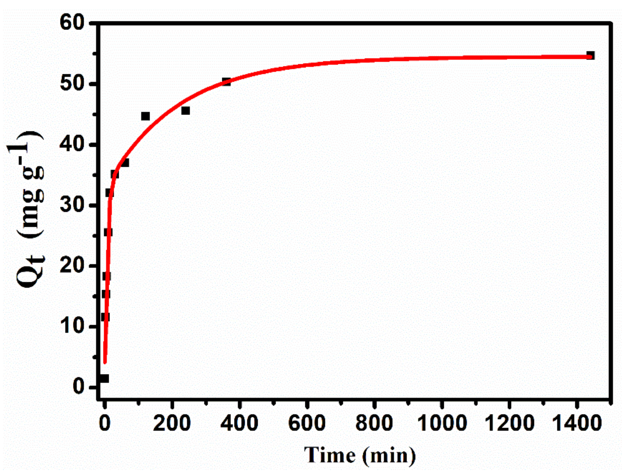

Fig. S25. Adsorption kinetics of $Cr_2O_7^{2-}$ in Hf-MOF-2 with an initial concentration of 50 ppm.

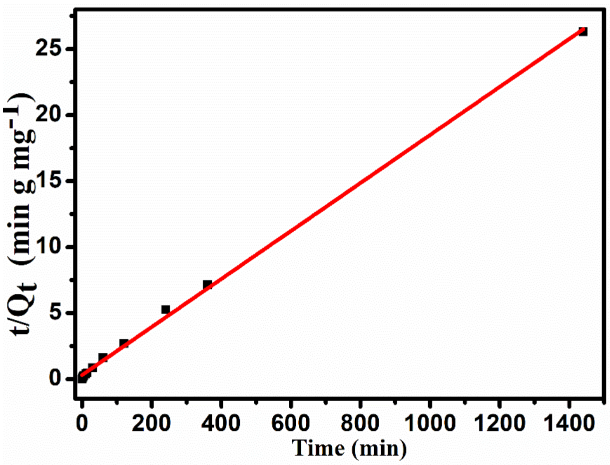

Fig. S26. The pseudo-second-order kinetic plot for the adsorption of $Cr_2O_7^{2-}$ in Hf-MOF-2.

References

1. Y. Jiang, L. Sun, J. Du, Y. Liu, H. Shi, Z. Liang and J. Li, *Cryst. Growth Des.*, 2017, **17**, 2090-2096.
2. L. Zhang, B. Guo, H. He, X. Zhang, Y. Feng, W. Fan, J. Cao, G. Lu, Y. Chen, D. Sun and W. Huang, *Inorg. Chem.*, 2020, **59**, 695-704.
3. J. Liu, Y. Ye, X. Sun, B. Liu, G. Li, Z. Liang and Y. Liu, *J. Mater. Chem. A*, 2019, **7**, 16833-16841.
4. J.-M. Liu, J.-X. Hou, J. Liu, X. Jing, L.-J. Li and J.-L. Du, *J. Mater. Chem. C*, 2019, **7**, 11851-11857.